19th Brazilian Congress of Thermal Sciences and Engineering
November 06th-10th, 2022, Bento Gonçalves - RS - Brazil

ENC-2022-0196
THREE-DIMENSIONAL CFD INVESTIGATION OF THE SIDEWALL COMPRESSION ANGLE IN A SCRAMJET INTAKE

João Vitor Marques Brito de Siqueira
Guilherme Borges Ribeiro
Instituto de Tecnológico de Aeronáutica - Praça Marechal Eduardo Gomes, 50 - Vila das Acacias, São José dos Campos - SP, 12228-900
Joaovitormarques22@hotmail.com, guiborgesribeiro@gmail.com

Abstract. *During the 21st century, a great number of loads are assumed to be taken into orbit. The cost to put something into orbit is enormous and therefore the development of an air-breathing engine as an alternative for hypersonic propulsion is required. Scramjet (supersonic combustion ramjet) engines are often seen as a promising alternative to place payloads in the Earth's orbit. Such air-breathing engines have a simple structure and a few moving parts. Nevertheless, developing a scramjet intake is not a trivial task. High heat fluxes and pressure loads on the walls, shock-wave-boundary-layer interactions, and the risk of chocked flow inside the isolator channel are a few examples of obstacles that need to be addressed during the scramjet design. This way, this work has the purpose of investigating the effects of sidewall compression inside the isolator. Computational Fluid Dynamics (CFD) simulations regarding the entire scramjet intake for the same flight conditions but varying the sidewall compression angle have been carried out. Mach number contour shows that the greater the compression angle the bigger the boundary layer separation near the upper wall. Yet this work investigated the effects of varying the sidewall compression angle on the scramjet performance parameters. Results in this work suggest that the higher the compression angle the lower the pressure recovery factor and the isentropic efficiency, which means the scramjet intake becomes less effective. However, this work shows that the sidewall compression in this analysis is an alternative to deal with the high pressure peak on the upper wall of the isolator. By fine-tuning the compression angle it is possible to decrease the pressure peak and also change its location to avoid a possible damaging-structure scenario.*

Keywords: *Scramjet, CFD, Sidewall Compression*

1. INTRODUCTION

During the 21st century, a great number of loads are assumed to be taken into orbit. The cost to put something into orbit is enormous and therefore the development of an air-breathing engine as an alternative for hypersonic propulsion is required. The great advantage air-breathing engines have is that they don`t need the vehicle itself to transport the oxygen for the combustion, as it happens to rocket engines. The use of air-breathing engines enables the vehicle to decrease its volume and weight resulting in higher specific impulses (Heiser, 1994; Segal, 2009; Griffiths, 2005; Smart, 2008; Alcaide, 2007). The supersonic combustion ramjet (scramjet) has been conceived to operate in high altitude flights. Its theoretical top speed is between Mach numbers 12 and 24 (Segal, 2009). The ramjet engine features combustion in subsonic flow while the scramjet engine has its fuel combustion happening with air at supersonic speed. That difference brings up some technological challenges to develop a scramjet engine. When the airflow is decelerated by the scramjet engine, the relative velocity and kinetic energy decrease, and conservation of energy requires that any missing kinetic energy will reappear as internal energy, with the result that pressure, temperature, and density of the flow entering the burner are considerably higher than in the freestream. When the flight Mach number exceeds about 6, this effect becomes so pronounced that it is no longer advantageous to decelerate the flow to subsonic speeds (Heiser, 1994). As in any conventional thermal power cycle, in both engines, the flow is compressed. The airflow compression is done by oblique shock waves at the inlet and diffuser. After such compression in ramjet engines, the airflow becomes subsonic after passing by a normal shock wave and inside the burner happens subsonic combustion. On the other hand, in scramjet engines, the airflow goes to the burner in supersonic speeds. If velocities are increased too much, the normal shock wave that occurs inside the ramjet engine leads to hugely high pressure loss. Yet the temperature increases a lot causing structural stresses and chemical dissociation of the airflow, which makes the cycle to lose energy (Smart, 2008). The solution for it is to remove the normal shock and allow the airflow to enter the combustor in supersonic speeds, from where comes the idea of the supersonic combustion ramjet, or scramjet. The fuel, in a scramjet engine, remains inside the burner for a really short time and therefore it is

injected just downstream the diffuser to achieve a rapid and thorough mixing. Thus, the high pressure, hot flow is directed to the nozzle that, in the case of a scramjet engine, must be divergent once the airflow is supersonic. The after-combustion flow is then exhausted into de atmosphere and can also be accelerated by the vehicle after-body that can be used as an expansion surface. Scramjets are supposed to operate in hypersonic speeds, i.e. above Mach 5, and theoretical operational limits as high as Mach 24 (Segal, 2009).

The scramjet, as well as other air-breathing propulsion systems, needs to operate at ideal altitudes to produce great dynamic pressure necessary for maximum performance. Relatively low altitudes, for long periods, are not the ideal for proper operation of the scramjet engine once high dynamic pressure and high Reynolds numbers can cause uncertainty in the boundary-layer transition, large aerodynamic loads, and a great surface heating. These are the phenomena that, in general, determine the design of the vehicle (Bertin, 1994). The scramjet engine needs to operate at hypersonic airflow so that the engine inlet can produce oblique shock waves that compress the airflow to enable combustion and ideal operation of the engine. Hence, the scramjet engine can't take off by itself. A turbojet engine can accelerate the hypersonic vehicle at speeds that make possible the scramjet to reach hypersonic speeds. For missions beyond the earth's atmosphere, rocket engines need to be activated (Segal, 2009).

The subsequent step in this work, is the 3D numerical analysis of the isolator of a scramjet engine. The isolator is part of a complete intake, which is composed by a forebody with three compression ramps (triple wedge) and an isolator. The advantage of three compression ramps is getting closer to an isentropic compression that maximizes the total pressure recovery inside the isolator (Heiser, 1994). This scramjet engine analyses considered 0.5 mm of forebody and cowl leading edge radii, isolator heights of 20 mm. Regarding the numerical details and boundary conditions, this work considered transitional viscous SST model, different wall conditions for the walls, 30 km of flight altitude and different sidewall compression angles inside the isolator. The sidewall compression in an isolator decreases the scramjet performance but can be an alternative to overcome engineering problems related to heat flux and pressures inside the isolator.

The desire for hypersonic flight in the atmosphere has driven many scientists and engineers throughout the years. In the late 1950s and 1960s, rocket engines were vastly used to access space, however, it was a common sense that only an airbreathing propulsion system would be able to provide a practical hypersonic flight cruise. The most suitable engine for this kind of flight is certainly the scramjet or supersonic combustion ramjet. The scramjet engine uses the shock waves generated at its intake to compress the airflow and enter the combustion chamber in supersonic velocities. The intake of scramjet engines plays an important role to enable efficient combustion and, therefore, has been extensively studied by many researchers in the last years. One of the main challenges in designing a scramjet intake is to obtain enough total pressure before the incoming airflow enters the combustion chamber. To accomplish it, freestream airflow is compressed by compression ramps (double or triple wedge) and also side-wall compression. Many researches have been carried out lately with the purpose of investigating the effects of sidewall compression. (Nguyen et al, 2013), for example, presented the numerical simulations and the performance analysis of a scramjet inlet as part of a combined experimental and numerical study. This work analyzed different angles of sidewall compression ramp, which took place in the double-wedge region. Heat flux and pressure on the walls are investigated. The numerical results in this work point out that the weak sidewall compression alters the inlet performance expressively. Although the static pressure is increased due to more compression, both the mass flow capture and the total pressure ratio are reduced. This is because the shock system has a tendency to deflect the flow upward and there are increased pressure losses due to stronger shock waves and larger separations. Another contribution in the sidewall compression ramp effects in a scramjet intake is the work done by (Hohn and Gülhan, 2011) where they presented the results of an extensive measurement campaign to investigate the effects of external and internal sidewall compression and the variation of internal contraction on the performance and flow field of a scramjet inlet. The investigations were conducted in the H2K wind tunnel of DLR, German Aerospace Center, at Mach 7. The analysis was based on static and total pressure ratios, kinetic energy efficiency, and mass capture ratios. The flowfield was analyzed using wall pressure distributions, pitot pressure, and Mach number profiles at the isolator interface to the combustion chamber and infrared thermography on the external ramps. Results showed that the external sidewall compression, combined to a two-ramp intake, is not suitable for increasing the inlet compression capability as it induces strong separation and vortex structures in the external part, which strongly increase spillage and impair the starting behavior. Considering the internal compression, results showed that there is significant increase of pressure ratio but at a high cost of total pressure losses.

Because of the adverse pressure gradient generated by shock-wave-boundary-layer interactions, the flow can be decelerated to subsonic speeds via normal shock. This leads to engine unstart of the engine including other undesirable phenomena such as high drag and increased localized heating. This work focuses on study, through computational fluid dynamics, how the change in cowl angle can help to prevent such phenomena. It was found that the increase of the angle of attack of the cowl decreases the size of boundary layer separation at the cost of a loss in total pressure and intake unsteadiness. Another worth mentioning work is the one from Siqueira (Siqueira et al., 2020). In this work, it was numerically examined the evaluation of effects of the isolator height and leading-edge bluntness on a scramjet intake. Hypersonic speeds make the temperature and heat flux to increase a lot on leading edges. In this way, the scramjet intake must feature blunt leading edges. This work considers three leading-edge radii: sharp, 0.5, and 1.0 mm. Besides it, isolator height was also investigated. Two heights were considered: 15 and 20 mm. It was evidenced that both leading-edge

bluntness and isolator height greatly influence the intake airflow structure. Results showed that the isolator height had a major effect on the flow separation at the isolator entrance yielding a recirculation zone that increases with the isolator height. Furthermore, higher Stanton numbers and temperature along the isolator were found for the shorter isolator height due to stronger shock waves and higher frequency of shock-wave train. Regarding the analysis of the leading-edge bluntness, Siqueira (Siqueira et al., 2020) found out that the heat flux decreases on the leading edges as the radius increases. Nevertheless, a decrease in the adiabatic kinetic efficiency was observed when the leading-edge radius was increased. Moreover, blunt leading edges promoted a decrease in heat flux along the scramjet intake walls and also a decrease in average temperatures throughout the isolator. One last example is of state-of-art research in developing scramjet intakes is the work proposed by Zhu (Zhu et al, 2018) that designed a three-dimensional hypersonic inward-turning intake with tri-ducts for combined cycles engines for the operation of three different modes controlled by a single rotational flap on the compression side, which efficiently simplifies the inlet structure and the flap control mechanism. At high flight speed between Mach 4 and 6, the pure scramjet mode is switched on, whereas both the ejector and the scramjet paths are open for a moderate Mach number between 2 and 4 with a larger throat area guaranteeing the inlet startability. In the low flight speed range with Mach number below 2, the additional turbojet path will be turned on to provide air for the turbine engine, whereas the other two paths remain open for spillage. Results show that numerical simulations under different operation modes have proven the utility and good performance of the designed inlet. It could be stated because of a nearly full mass flow ratio and a total pressure recovery of around 0.5 that could be achieved at the cruise speed. Meanwhile, the intake works correctly at low flight speeds which overcomes the typical starting problem seen in intake designs.

In this scenario, the present work contributes to the state-of-art development of a scramjet intake by analyzing, through 3D CFD analysis, the effects of the change related to the isolator sidewall compression angles. This work focus on the change in sidewall compression angles has on performance. Contour images and values of properties along the walls were considered in the analyses. Five compression angles were examined: 0°, 4°, 6°, 8° and 10°. The flight condition is the same for all cases: 30 km of altitude at Mach 6.8. Results show that the most prominent consequence of an increase in compression angle is that the intake decreases its performance. Results also show that by changing the compression angle it is possible to position the pressure peaks in different locations along the upper wall of the isolator. That can be seen as an engineering solution to overcome the high heat flux and pressure loads that exist inside the isolator

In this way, it is possible to state that this work gives its contribution to advance in this challenging field of designing an airbreathing engine to power hypersonic speed vehicles. All the numerical calculations in this work used the fluid dynamics ANSYS Fluent code. Therefore, the numerical methods and transitional viscous models used in this work were the ones available in Ansys Fluent (ANSYS, 2020).

2. MATHEMATICAL EQUATIONS

The classical Navier-Stokes equations for compressible flow has been considered. For a time-dependent fluid flow, Eq.(1) represents the mass balance, Eq.(2) to Eq. (4) the momentum balances in the x, y and z directions, and Eq. (5) is the energy balance. In these equations, *u, v, w* refer to flow velocities in the x, y and z directions respectively. And $\boldsymbol{u}$ represents the total vectorial flow velocity that is obtained from the sum of the contributions of x, y, and z. The term Φ refers to the dissipation function, represented by Eq. (6) and μ is a viscosity term that relates the stresses to the volumetric deformation. And finally to close the set of equations it is considered the ideal gas law equation – Eq. (7) – where *R* refers to the ideal gas constant.

$$\nabla.(\rho \boldsymbol{u}) = 0 \tag{1}$$

$$\nabla.(\rho u \boldsymbol{u}) = -\frac{\partial p}{\partial x} + \nabla.(\mu \nabla u) + S_{Mx} \tag{2}$$

$$\nabla.(\rho v \boldsymbol{u}) = -\frac{\partial p}{\partial y} + \nabla.(\mu \nabla y) + S_{My} \tag{3}$$

$$\nabla.(\rho w \boldsymbol{u}) = -\frac{\partial p}{\partial z} + \nabla.(\mu \nabla w) + S_{Mz} \tag{4}$$

$$\nabla.\left(\rho c_p T \boldsymbol{u}\right) = -p\nabla.\boldsymbol{u} + \nabla.(k\nabla \mathrm{T}) + \Phi + S_i \tag{5}$$

$$\Phi = \mu\left\{2\left[\left(\frac{\partial u}{\partial x}\right)^2 + \left(\frac{\partial v}{\partial y}\right)^2 + \left(\frac{\partial w}{\partial z}\right)^2\right] + \left(\frac{\partial u}{\partial y} + \frac{\partial v}{\partial x}\right)^2 + \left(\frac{\partial u}{\partial z} + \frac{\partial w}{\partial x}\right)^2 \left(\frac{\partial v}{\partial z} + \frac{\partial w}{\partial y}\right)^2\right\} + \lambda(\nabla.\boldsymbol{u})^2 \tag{6}$$

$$p = \rho R T \tag{7}$$

The previous equations, written in differential form, describe energy, momentum and mass flow within an infinitesimal. Because of the turbulent nature of the flow, the solver used in this work considers and adapted version of these equations. The turbulence model used in the calculations to solve the turbulence closure problem presented in this work is transition SST. The transition SST model is based on the coupling of the SST $k-\omega$ transport equations with two other transport equations, one for the intermittency γ and one for the transition onset criteria.

The total pressure recovery is the ratio of the average total pressure at the isolator exit of the intake to the freestream total pressure. A higher total pressure factor indicates a better performing intake. The maximum possible value of recovery is 1.0. It is calculated as follows

$$PRF = \frac{P_1}{P_\infty}\left(\frac{1+\frac{\gamma-1}{2}.M_1^2}{1+\frac{\gamma-1}{2}.M_\infty^2}\right)^{\frac{\gamma}{\gamma-1}} \tag{7}$$

where P_∞ and P_1 are the pressures of the freestream and inlet exit respectively. γ is the freestream heat capacity ratio and M_∞ and M_1 are the Mach numbers of the freestream and inlet exit, respectively. P_1 and M_1 were obtained through mass-weighted-average values considering the integral of the isolator exit surface.

Yet, another performance parameter considered in this work is the isentropic efficiency η, which is calculated as follows

$$\eta = \frac{H_{1s}-H_\infty}{H_1-H_\infty} \tag{8}$$

where H_∞ and H_1 are the freestream and isolator exit enthalpies. H_1 was also obtained through mass-weighted average value considering the integral of the isolator exit surface. H_{1s} is the isolator exit enthalpy for an isentropic process, which is obtained as follows

$$H_{1s} = H_\infty\left(\frac{P_1}{P_\infty}\right)^{1-\frac{1}{\gamma}} \tag{9}$$

where H_∞ is the freestream enthalpy, P_∞ and P_1 are the freestream and isolator exit pressures. γ is, as expected, the freestream heat capacity ratio. P_1 was obtained through mass-weighted average value considering the integral of the isolator exit surface.

In order to solve the Navier-Stokes equations and all other transport equations the commercial software Ansys Fluent used the finite volume method. Therefore a mesh must be created to obtain the partial differential equations in the algebraic format. Figure 1 shows the vehicle leading edge of mesh considered in this calculation. For all meshes, a region along the compression ramps and isolator up to a distance of 5 mm plus the radius from the wall is considered to be more refined to properly capture the viscous effects inside the boundary layer and its relation with shock waves in the intake. Regarding the refinement on the Z-axis, a region 15 mm from the sidewall is chosen to have more refined elements. An exponential size growth is considered in these regions such as, closer to the wall, more refined elements are found. The meshes all features around 14 million hexahedral cells.

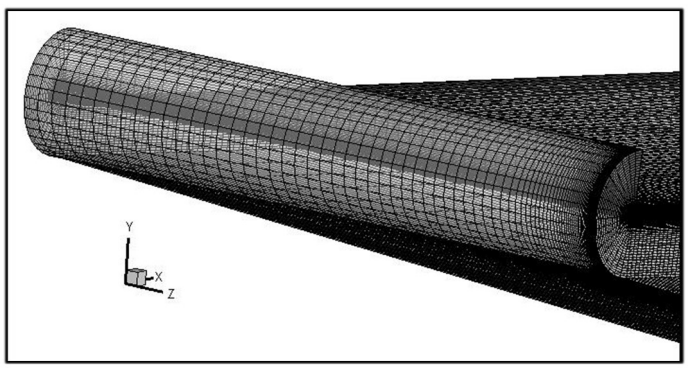

Figure 1 - Detailed parts of the mesh of the vehicle leading-edge.

3. ANALYSIS OF THE SIDEWALL COMPRESSION VARIATION

This work's goal is to investigate the effects of sidewall compression in a scramjet intake considering different compression ramp angles. More precisely, 4 angles were analyzed: 4, 6, 8 and 10 degrees. All cases considered the freestream related to a 30 km flight at Mach number 6.8 and with no AoA. Yet a case without sidewall compression has been considered when analyzing the performance parameters. The compression of this analysis is related to the isolator sidewall. The isolator cross-sectional area gradually reduces as the isolator compression angle increases. The sidewall ramp starts at the isolator inlet and extend 40 mm in the x-axis along the isolator for all 4 cases, as it was shown in Figure 3. Figure 2 shows the computational domain of the entire scramjet intake. As can be seen, the greater the angle of the compression ramp, the narrower the isolator after the sidewall compression. The analyses present in this work considers contour images of Mach number, distribution of pressure on the upper wall and along the compression ramp, and analysis of performance parameters, as have been discussed in this work.

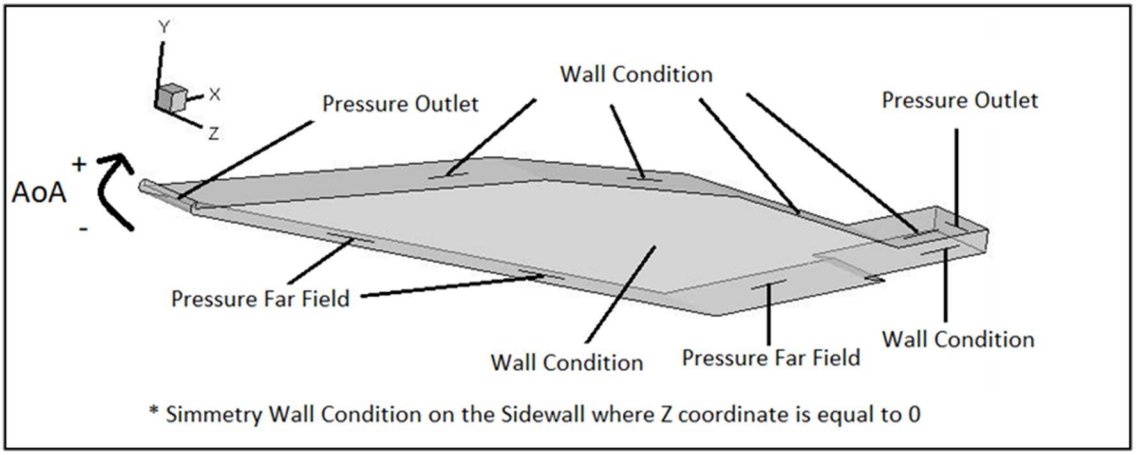

Figure 2 – Computational domain of the scramjet intake.

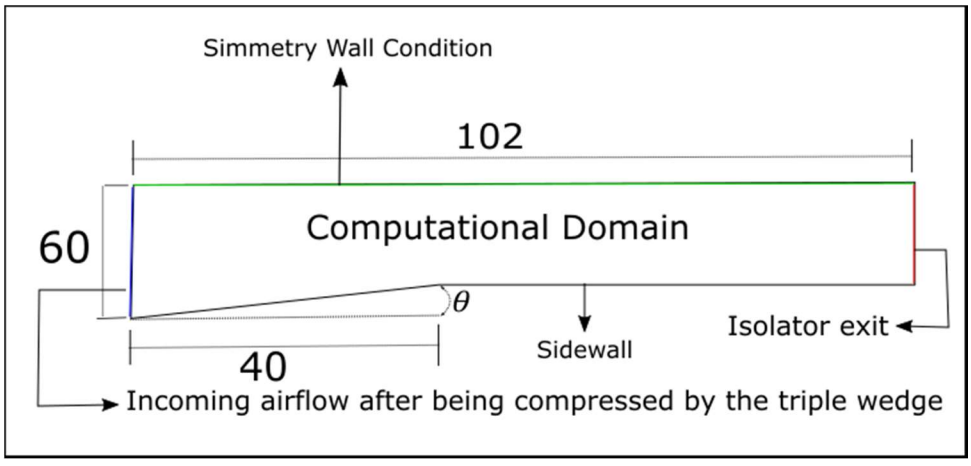

Figure 3 - Top view of the isolator considering sidewall compression (mm).

Contour images of Mach number – Figure 4 until Figure 8 - are displayed in this subsection considering different sidewall compression angles. The incoming airflow analyzed has already been compressed by the triple wedge and, as soon as it enters the isolator, it is influenced by the sidewall compression. An effect of this compression, observed in these results, is the small increase of the boundary layer separation near the upper wall of the isolator as the compression angle increases. Very complex shock-wave-boundary-layer interactions, whose analysis is not part of the scope of this work, takes place in the beginning of the isolator. Having another flow compression in this region certainly affects the shock-wave structures and increases the irreversabilities in this region. More irreversabilities is generated by a greater boundary layer separation. Results show that there is a low Mach number region on the lower wall which is very little influenced by the sidewall compression along the entire isolator.

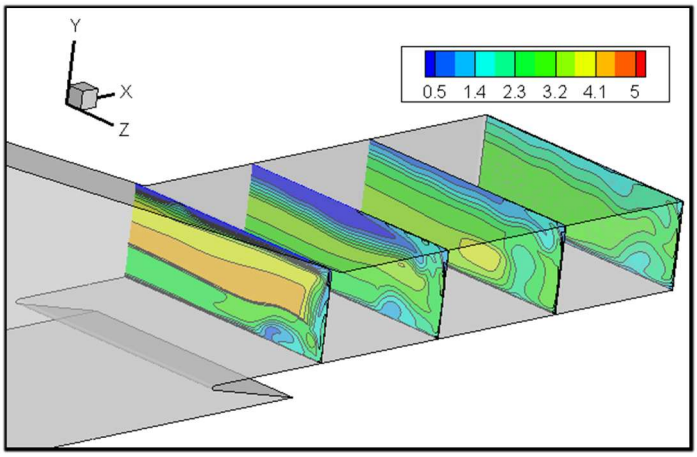

Figure 4 – Mach number contour of an isolator featuring no sidewall compression.

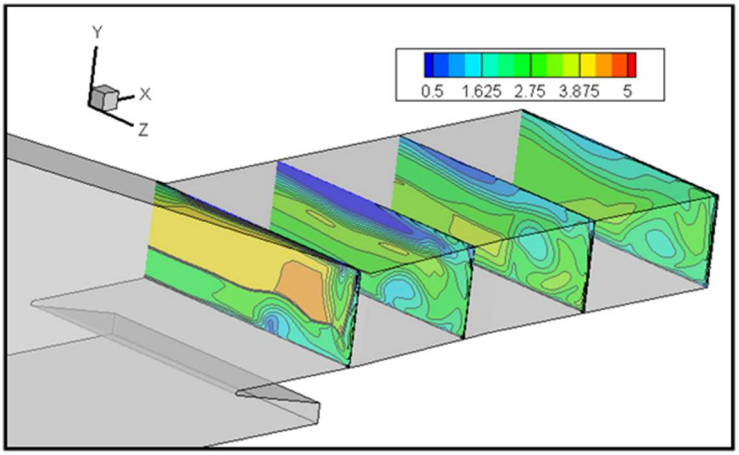

Figure 5 – Mach number contour of an isolator featuring 4° of sidewall compression.

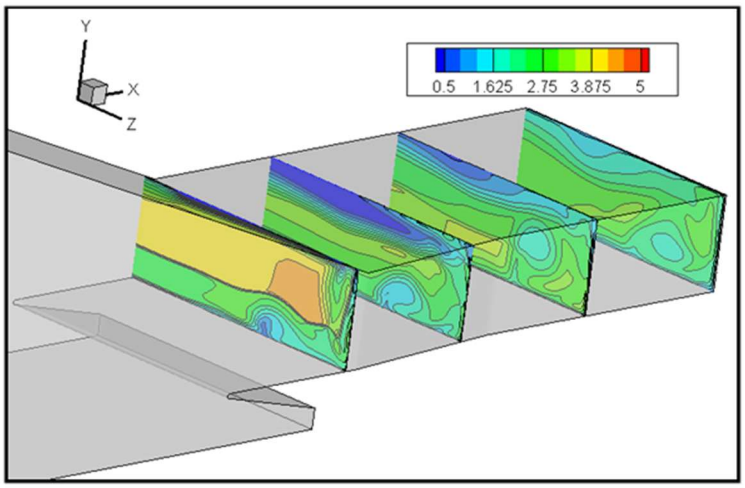

Figure 6 - Mach number contour of an isolator featuring 6° of sidewall compression.

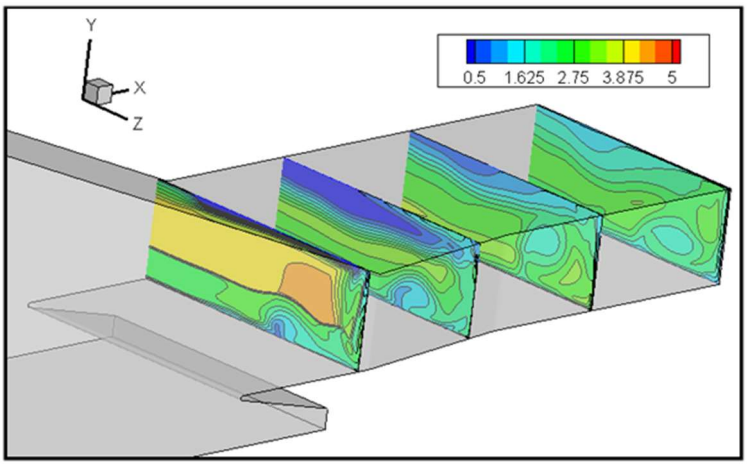

Figure 7 - Mach number contour of an isolator featuring 8° of sidewall compression.

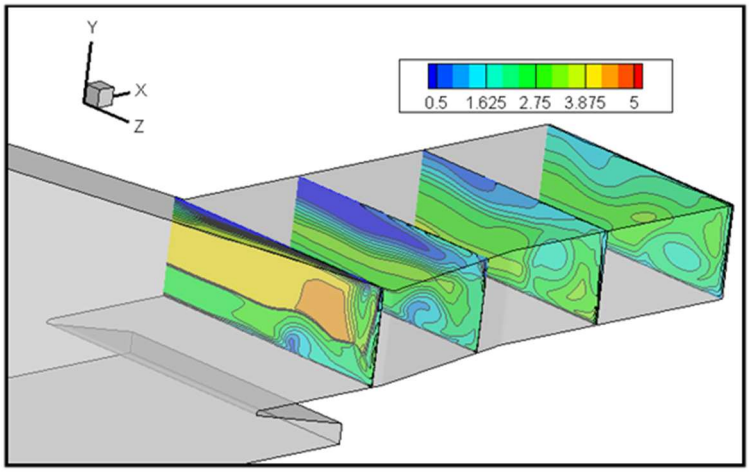

Figure 8 - Mach number contour of an isolator featuring 10° of sidewall compression.

Besides the contour analysis, this subsection also investigates the distribution of total pressure along the upper wall. The line on which this distribution is considered is at z = 0 mm, the farthest possible from the sidewall. Results seen on Figure 9 shows that the pressure increases on the upper wall as the sidewall compression angle increases along the first 60 mm, just before the pressure peak where the reflected shock-wave impingement on the upper wall takes place. After the shock-wave impingement, the higher the compression angle the lower the pressure until the isolator exit. As the compression angle increases, the incoming airflow is directed more toward the inside of isolator and, as a result, the shock-wave impingement position, as well as the pressure peak, changes. The increase of the compression angle then makes the pressure peak to happen in a shorter distance along the x-axis. As suggested by the contour analysis, the higher the compression angle, the more irreversabilities in the airflow, explaining the higher pressure peaks on cases with lower compression angles. In addition, the high total pressures on the upper wall of the isolator are related to the dynamic pressure of the incoming airflow which is related to the airflow velocity. A higher compression angle represents a more direct impact of the airflow on the sidewall ramp. That makes the airflow velocity to decrease and, as result, the reflected shock wave total and its resulting pressure peak on the upper wall also reduces. At last, the lower pressure in the beginning of the isolator is related to the boundary layer separation, which is a low-pressure region by itself.

Scramjet intakes are likely to face extremely high pressure loads on the walls. Knowing that the isolator sidewall compression not only decreases the value of the pressure peak on the upper wall, but also changes its location, can certainly help during the design of a scramjet intake. The isolator sidewall compression can be used to distribute and handle more properly the high pressure loads inside the isolator. Without the isolator sidewall, the pressure peak location and intensity on the upper wall depends only on the freestream conditions.

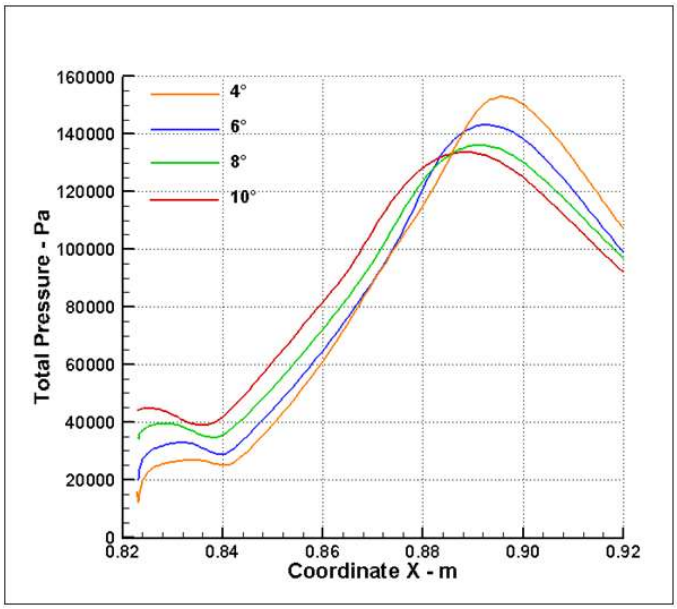

Figure 9 – Total pressure distribution along the upper wall considering different sidewall compression angles.

For measuring the intake performance considering the sidewall-compression-angle variation, it was considered the pressure recovery factor (PRF) and the isentropic efficiency. Remembering that both parameters relate the actual airflow at the intake exit with an airflow whose origin is an isentropic process and therefore, these parameters can provide an insight of how much entropy is generated and consequently how efficient are the geometries. Results seen on Figure 10 and Figure 11 show that the increase of the sidewall compression angle analyzed in this subsection influences little both performance parameters. Actually, in comparison with a case without sidewall compression – red bar on both Figures – results suggest that this sort of sidewall compression inside the isolator makes the intake to be less performing. Having another compression ramp at that region certainly generates lots of irreversabilities when another reflected shock wave, originated in this new compression, is added to an already very complex airflow structure which interacts reflected shock waves with boundary layers in a viscous airflow with very high temperatures and pressures. This increase of irreversabilities resulted in increased boundary-layer separations – mainly on the upper wall – and decrease of the overall intake performance. This analysis is in accordance with the calculation of entropy generation, presented in the following subsection.

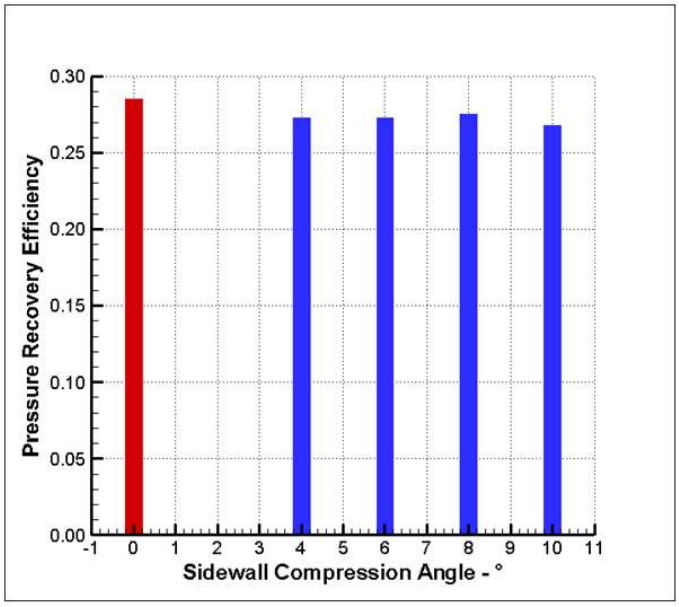

Figure 10 - Pressure recovery factor of the intake for different sidewall compression angles.

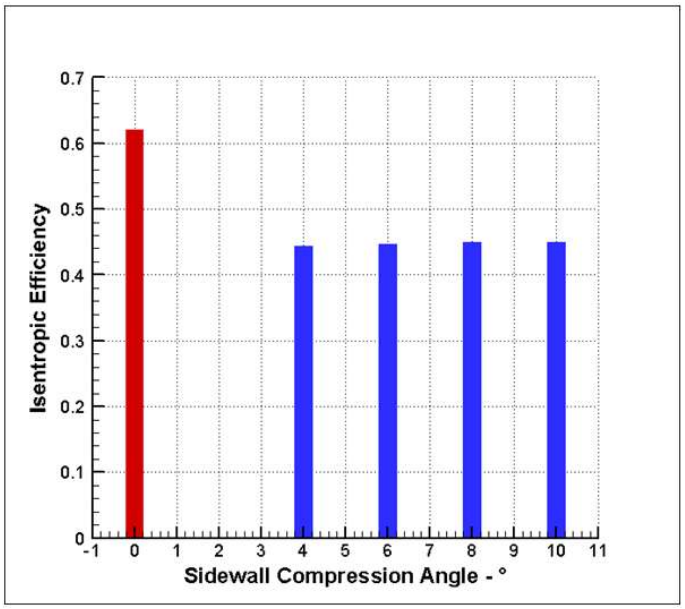

Figure 11 – Isentropic efficiency of the intake for different sidewall compression angles.

4. CONCLUSIONS

This work showed that the higher the compression angle the greater the boundary layer separations, which causes more irreversabilities that leads to a decrease of performance. The main discussion of this work is the isolator sidewall compression as an engineering solution to deal with problems such as high pressure peaks inside the isolator. By fine-tuning the compression angle it is possible to decrease the pressure peak as well as its location on the upper wall of the scramjet isolator. Results shown in this analysis indicate that the cost of applying such solution is to have a less performing intake. Certifying that there will be no structural damage to the scramjet engine is one of the parameters taken into account when defining the flight envelope of a hypersonic vehicle. Therefore, sidewall compression can offer alternatives to deal with the high pressure peaks inside the isolator, and that can be determinant to extend the limits of the flight envelope of a hypersonic vehicle, at the cost, however, of having a less performing intake and consequently an engine. Results in this subsection have shown, nevertheless, that once there is sidewall compression, varying its compression angle will not significantly impair the intake performance.

5. ACKNOWLEDGEMENTS

This work is part of a longstanding research program supported by the Brazilian Air Force. The technical support of the Institute of Advanced Studies (IEAv) is highly acknowledged as well the financial support provided by CAPES.

6. REFERENCES

ALCAIDE, R. L. M. **Investigação da Combustão Supersônica em Túnel de Choque Hipersônico**. 2007.97f. Thesis (Master in Science) – Instituto Tecnológico de Aeronáutica, São José dos Campos.

ANSYS, ANSYS Fluent 19.0 user's guide, Canonsburg, 2018.

BERTIN, J.J. **Hypersonic aerothermodynamics.** Washington, DC: AIAA, 1994. 608 p. (AIAA education series).

GRIFFITHS, A. D. **Development and Demonstration of a Diode Laser Sensor for a Scramjet Combustor**. 2005. Thesis (Doctor of Philosophy) – The Australian Natonal University, Australia.

HEISER, W. H.; PRATT, D. T. **Hypersonic Airbreathing Propulsion**. Reston, VA: AIAA, 1994.

HOHN O., GULHAN A. Experimental Investigation on the Influence of Sidewall Compression on the Flowfield of a Scramjet Inlet at Mach 7. *In* 17th AIAA INTERNATIONAL SPACE PLANES AND HYPERSONIC SYSTEMS AND TECHNOLOGIES CONFERENCE. 2011, San Francisco, USA. **Proceedings…** American Institute for Aeronautics and Astronautics (AIAA), 2011. doi:10.2514/6.2011-2350.

NGUYEN, T., BEHR, M., REINARTZ, B., HOHN, O., & GULHAN, A. Effects of Sidewall Compression and Relaminarization in a Scramjet Inlet. **Journal of Propulsion and Power**, 29(3), p.628-638. 2013. doi: 10.2514/1.b34740.

SEGAL, C. **The Scramjet Engine: Process and Characteristics**. 1st ed. Cambridge: Cambridge University Press, 2009. 270 p.

SMART, M. Scramjets. In: **NATO/OTAN.RTO-EN-AVT-150**, Neuilly-sur-Seine, France: RTO, 2008, p. 1–38.

SIQUEIRA, J. V. M. B., ROSA, M. A. P., RIBEIRO, G. B. Numerical evaluation of effects of the isolator height and the leading-edge bluntness on a scramjet inlet. **Journal of the Brazilian Society of Mechanical Sciences and Engineering**, 42(6). 2020.

ZHU, C., Zhang, X., Kong, F., & You, Y. (2018). **Design of a Three-Dimensional Hypersonic Inward-Turning Inlet with Tri-Ducts for Combined Cycle Engines**. In: *International Journal of Aerospace Engineering, 2018, 1–10.*

7. RESPONSIBILITY NOTICE

The author(s) is (are) the only responsible for the printed material included in this paper.